

Wide Field X-Ray Telescope Mission

A white paper submitted in Response to Solicitation NNH11ZDA018L

PI: Stephen S. Murray Johns Hopkins University, Physics and Astronomy Baltimore MD 21218

Phone: (410) 516-2335 Email: ssm@pha.jhu.edu

Riccardo Giacconi, Timothy Heckman, Kip Kuntz, Suvi Gezari Johns Hopkins University

Hal Weaver, Carey Lisse, Neil Miller, Cheryl Reed Applied Physics Lab

Alexey Vikhlinin, William Forman, Christine Jones, Andrew Goulding, Paul Reid,

Andreas Zezas, Pepi Fabbiano Harvard-Smithsonian Center for Astrophysics

Martin Weiskopf, Brian Ramsey, Ron Elsner, Steve O'Dell Marshall Space Flight Center

Andrew Ptak Goddard Space Flight Center

Mark Bautz Massachusetts Institute of Technology

Ryan Hickox Dartmouth College

Niel Brandt, Eric Feigelson, Don Schneider The Pennsylvania State University

Neta Bahcall Princeton University

Steve Allen Stanford University

Megan Donahue, Mark Voit Michigan State University

Gus Evrard University of Michigan

Kathryn Flanagan, Carol Christian Space Telescope Science Institute

Andrey Kravtsov University of Chicago

Brian McNamara University of Waterloo

Piero Rosati, Paolo Padovani European Southern Observatory

Rashid Sunyaev Max Planck Institute for Astrophysics

Stefano Borgani University of Trieste

Maurizio Paolillo University of Naples Federico II

Giovanni Pareschi, Oberto Citterio, Gianpiero Tagliaferri, Sergio Campana, Ginevra

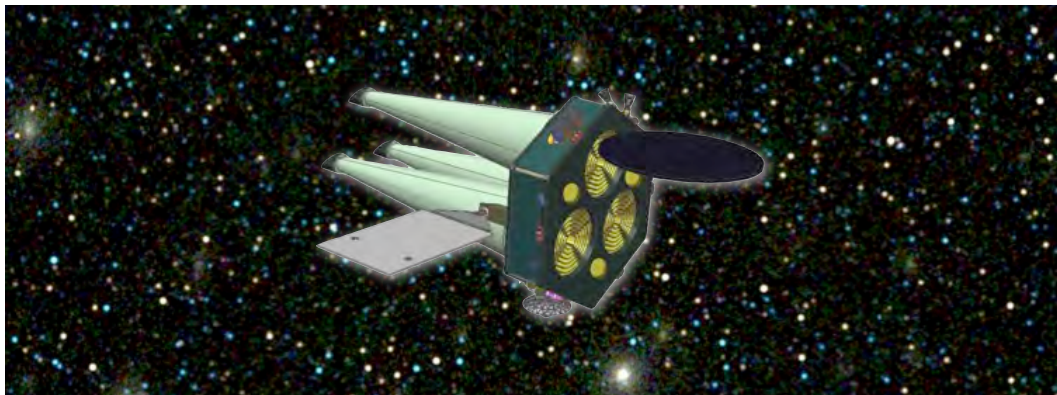
Trinchieri, Marta Civitani, Alberto Moretti INAF-Astronomical Observatory of Brera

Roberto Gilli INAF-Astronomical Observatory of Bologna

Paolo Tozzi, Joana Santos, Barbara Sartoris INAF-Astronomical Observatory of Trieste

Massimo Della Valle, Domitilla de Martino INAF- Astronomical Observatory of Capodimonte

Paolo Giommi ASI Science Data Center



- **WFXT is moderate cost; < \$1B including reserves, launch, operations and GO program.**
 - Validated by Independent Cost Estimate; \$779M with reserves, exclusive of launch (\$90–180M)
- **WFXT is technically ready to start now and launch in 5.5 years**
 - Mission design has large mass (~30%) and power (~80%) margins above standard contingencies
 - TRL > 6, except for telescope currently at TRL 4 with ongoing development already in place to achieve TRL 5 in this calendar year and TRL 6 by the end of Phase A.
- **WFXT addresses RFI and NWNH Science Objectives, for example:**
 - Growth and Evolution of Supermassive Black Holes and Feedback
 - Formation and Evolution of Clusters of Galaxies and Cosmology
 - Growth of Large Scale Structure and the Cosmic Web

Executive Summary

Exploring the high-redshift Universe to the era of galaxy and cluster formation requires an X-ray survey, which matches in *sky coverage, sensitivity and angular resolution* the current and next generation of wide-area optical surveys, such as Pan-STARRS and LSST, in the near-IR (e.g. Euclid, WFIRST), as well as at submm and radio wavelengths (CCAT, SKA). The vast scientific potential of these survey missions from the optical through the radio has been recognized by the 2010 Decadal Survey “New Worlds, New Horizons in Astronomy and Astrophysics” [1]. X-ray observations are key to a full synergetic exploitation of these future multi-wavelength data sets, as they have the unique ability to probe phenomena and unveil sources powered by gravity.

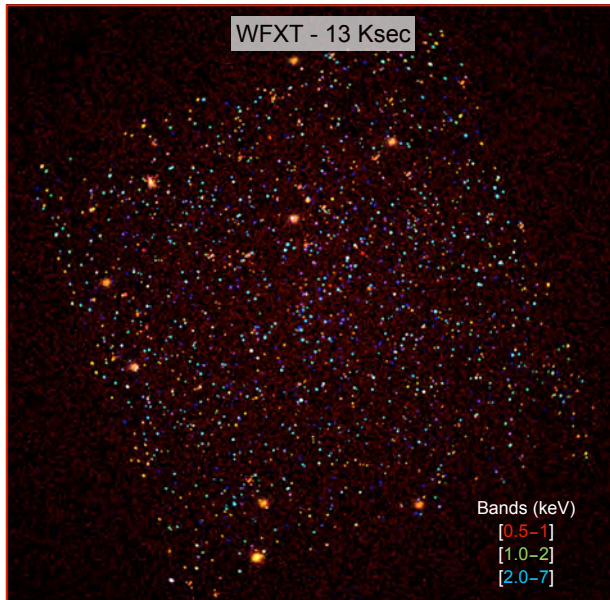


Figure 1: Simulated WFXT 13 ksec exposure of the COSMOS field constructed from the COSMOS catalog of AGN and clusters [8]. WFXT achieves in ~ 13 ksec the same sensitivity and sky coverage that required ~ 1.8 Msec of Chandra time, with comparable average PSFs ($5''$ vs $3''$).

To this end, we present the Wide Field X-Ray Telescope (WFXT) [2, 3, 4, 5, 6, 7], designed to be orders-of-magnitude more effective than previous or planned X-ray missions in carrying out surveys. This moderate class mission provides an affordable and essential tool for obtaining a unique astrophysical data set that will support contemporaneous and planned ground-based giant optical telescopes, ALMA, and on-orbit facilities, such as JWST. With a $5''$ angular resolution across a 1 deg^2 field of view, WFXT provides prompt and reliable multi-wavelength source identifications. In addition to a core survey program (see Fig.1 and Table 1), WFXT will provide a vigorous

guest observer (GO) program that allows targeted observations of peer selected fields for detailed study.

The proposed surveys will detect essentially all extended X-ray sources associated with massive virialized clusters to $z \lesssim 2$, with thousands of clusters at $z > 0.5$ bright enough for direct temperature and Fe-line redshift measurements. Large numbers of AGN will be discovered, including a sample of $\gtrsim 10^3$ high redshift sources ($z > 6$) that will probe the growth of black holes at the dawn of the galaxy formation era.

These data sets directly address key scientific objectives of NWNH, including those noted in Table 1 of the RFI regarding: the formation and evolution of clusters of galaxies and associated implications for cosmology and fundamental physics (*e.g.*, the nature of dark matter, dark energy and gravity); the growth of large scale structure in the Universe; black-hole formation and evolution; and AGN interaction with ICM and ISM. WFXT will also address other NWNH science objectives such as star formation; the high-energy stellar component and hot-phase interstellar medium of galaxies; the impact of X-ray flares in planet formation; and transient and variability behavior of cosmic sources (time domain studies).

Table 1: **WFXT survey parameters (0.5-2.0 keV)**

Quantity	Survey	
	Deep	Medium
$\Omega \text{ (deg}^2\text{)}$	100	3000
Exposure/deg 2	400 ksec	13 ksec
Total Time	1.5 yr	1.5 yr
$S_{\text{min point}} (S/N > 3)$ erg s $^{-1}$ cm $^{-2}$	4.0×10^{-17}	4.5×10^{-16}
Tot. AGN	$\sim 4.7 \times 10^5$	$\sim 4.4 \times 10^6$
$S_{\text{min extended}} (S/N > 5)$ erg s $^{-1}$ cm $^{-2}$	1×10^{-16}	1×10^{-15}
Tot. Clusters/Groups	$\sim 3 \times 10^4$	$\sim 2 \times 10^5$

WFXT is optimized for imaging performance over its full field of view, rather than mainly on-axis as with previous or planned surveys. Surveys will be carried out efficiently, and studies of targeted areas are typically covered by a single pointing. The technology to meet the science objectives is in hand, requirements on the launch vehicle and spacecraft are well within standard capabilities. WFXT is for the entire astronomical community. Data from the surveys will be publicly available in yearly releases. These data will be a legacy for numerous multi-waveband studies that will revolutionize astronomy. GO data after a short proprietary time consistent with NASA policies will become public via the WFXT data archive, and ultimately via the Multimission Archive at the STScI (MAST).

1 Mission Science

One of the great successes of the past decade was the Sloan Digital Sky Survey (SDSS) [9]. An X-ray equivalent is needed to survey the large volumes required to identify significant populations of both high redshift active galactic nuclei (AGN) and clusters of galaxies back to early epochs. Such surveys address fundamental questions raised in the 2010 Decadal Survey report [1] related to galaxy and black hole growth, the evolution of clusters of galaxies, the growth of large scale structure in the Universe, and also serve as target finders for future, more sensitive, but narrow field missions.

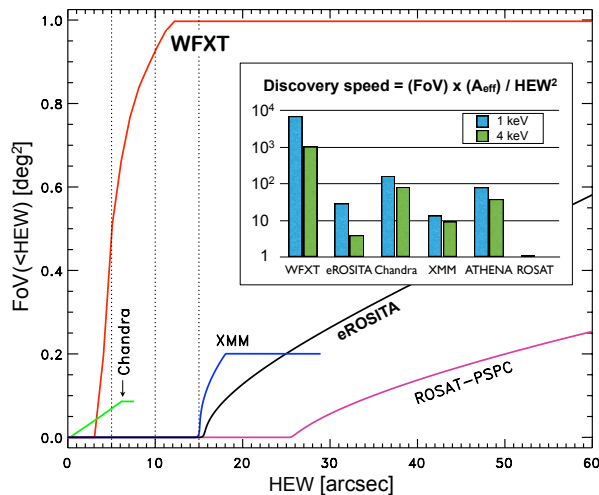


Figure 2: Cumulative field of view available at a given angular resolution (HEW) as a function of HEW for five missions. The insert shows the figure of merit for survey discovery speed ($\text{Grasp}/\text{HEW}^2$). WFXT is about two order-of-magnitudes better than any past or planned X-ray mission in carrying out large sensitive surveys and identifying distinct sources.

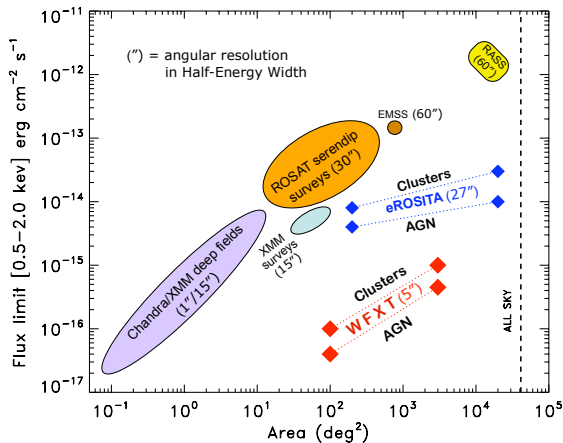


Figure 3: Effective flux limits and sky coverage for past and planned X-ray surveys. WFXT provides an unsurpassed combination of sensitivity and sky coverage.

The WFXT telescopes have an effective area of $\sim 0.7 \text{ m}^2$ at 1 keV and of $\sim 0.2 \text{ m}^2$ at 4 keV (~ 10 times larger than Chandra), with an average angular resolution (HEW) of $5''$ over a $1^\circ \times 1^\circ$ FOV. This resolution maximizes detection sensitivity, avoids source confusion, enables us to distinguish between clusters and AGNs at any redshift, and allows efficient and reliable follow-up identifications at other wavelengths. Moderate resolution spectroscopy, even for faint sources, allows us to broadly characterize their physical nature. Survey efficiency is characterized by the product of the collecting area A_{eff} , the effective field of view at the desired resolution $\text{FoV}(<\text{HEW})$, and the effective time available for observation T . The speed at which large areas are surveyed at a given depth and distinct sources are identified scales as $(A_{\text{eff}} \times \text{FoV})/\text{HEW}^2$ (Fig.2). WFXT maximizes this figure of merit by use of a wide-field optics design that is no greater in complexity than a traditional Wolter-I telescope. At an angular resolution of $5''$, the WFXT optic provides a field of view ~ 10 times larger than Chandra's. Combined with its larger effective area, WFXT will be $\gtrsim 50$ times faster than Chandra in surveying a square degree to a comparable flux limit and resolution, enabling large area deep surveys over large cosmologically interesting volumes.

The core program of extragalactic surveys will use about 60% of the nominal 5 year mission lifetime. It includes deep surveys to the flux limit of the Chandra Deep Field (4.0×10^{-17} and $1 \times 10^{-16} \text{ erg s}^{-1} \text{ cm}^{-2}$ for point sources and extended sources respectively) covering a total of $\sim 100 \text{ deg}^2$ (10 areas of 10 deg^2 each), ~ 1000 times the CDFS area; and a medium survey to a flux limit of 4.5×10^{-16} and $1.5 \times 10^{-15} \text{ erg s}^{-1} \text{ cm}^{-2}$ over $\sim 3000 \text{ deg}^2$ (Tab.1, Fig.3). All of the survey data will be made public through a series of annual Data Releases. WFXT allocates 40% of the mission to a GO program, which will enhance the main survey area with complementary fields. GO data will include a short proprietary time before becoming public.

The public archive (an X-ray analog to the SDSS) will fuel a broad range of research by the entire community for decades. The proposed surveys will detect essentially all massive clusters, or dark matter halos with $M > 10^{14} M_\odot$ to $z \lesssim 2$, and groups of galaxies ($M < 10^{13} M_\odot$) to $z \sim 0.2$, with thousands of clusters bright enough for accurate temperature and X-ray redshift measurements. Large numbers of AGN will be discovered, including a sample of $\gtrsim 10^3$ high redshift sources ($z > 6$) that will probe the growth of black holes at the dawn of the galaxy formation era.

The synergy of WFXT with multi-wavelength deep wide-area surveys will unleash the full potential of

these surveys to address many outstanding scientific questions for the next decade and will consolidate their immense legacy value. For example, the combination of WFXT gas measurements and LSST lensing measurements with high sensitivity Sunyaev-Zeldovich surveys (e.g., ACT and SPT-Pol, Planck, CCAT) will provide a complementary probe of ICM physics and cluster masses. WFXT will be an outstanding source of high redshift clusters and AGN for follow-up studies with JWST, ALMA, the next generation of giant (30m) ground-based telescopes, and future X-ray observatories (e.g., SMART-X, Gen-X). WFXT will enable time domain studies, discovering hundreds of transient and variable sources including faint GRB/XRFs, tidal disruption events and ULXs, opening up a new discovery space probing the properties of these phenomena over cosmic time.

1.1 Physics of Clusters of Galaxies

Galaxy clusters are systems where astrophysics and cosmology meet: while their overall internal dynamics are dominated by gravity, the cosmological processes taking place on very large scales leave observable imprints on the diffuse hot gas trapped within their potential wells [10, 11]. Over the last decade, observations with Chandra and XMM-Newton have led to important discoveries on the thermodynamics of the ICM in nearby, $z < 0.3$, clusters, while raising new outstanding questions: When and how is entropy (energy) injected into the intracluster medium (ICM)? What is the history of metal enrichment in the ICM? How is the emergence of proto-clusters at $z \sim 2$ related to the peak of star formation activity and black hole accretion?

WFXT will provide an efficient observational strategy to address these questions. Fig.4 shows the number of clusters expected from WFXT surveys, compared with the expectations for eROSITA [12]. For hundreds of these clusters, out to $z > 1$, there will be at least 15,000 detected counts, so that entropy as well as temperature maps will be measured with the precision currently achieved by Chandra and XMM for clusters at $z < 0.2$. The redshift evolution of the entropy structure of the ICM will shed light on when and how the excess energy was added to the ICM. Similarly, mapping the distribution of heavy elements in the ICM can be done for all clusters for which temperature profiles are measured. Measuring the global iron metallicity for hundreds of clusters to $z \sim 1.5$, will allow the history of metal enrichment to be determined, with far reaching implications for the star formation history in cluster environments. Finally the $\sim 50,000$ clusters discovered beyond $z = 1$

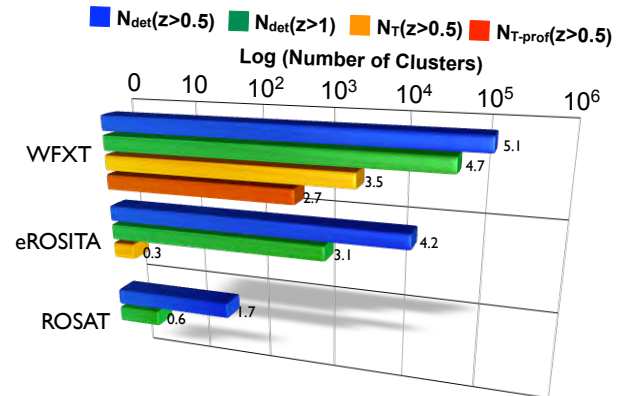


Figure 4: Number of clusters from (3-year long) WFXT surveys, compared with the eROSITA mission (2013) and the current ROSAT selected samples. Bars indicate the estimated number of clusters detected at $z > 0.5$ and $z > 1$ (with > 50 photon counts, blue and green respectively), number of clusters at $z > 0.5$ for which an accurate measurement of the temperature and redshift can be obtained (> 1500 counts; orange) and those at $z > 0.5$ for which temperature profiles and ICM metallicities can be recovered ($> 15,000$ counts; red).

will, for the first time, probe early stages of cluster formation when energy inputs from cluster mergers, supernova and AGN dominate the evolution of the intracluster medium. Characterizing the physical properties of these clusters will tell us how clusters form and evolve and will allow cluster scaling relations to be calibrated and used as robust tools to constrain cosmological parameters [10, 13].

1.2 Cosmology with Galaxy Clusters

The planned WFXT surveys will provide a vast sample of 200,000 galaxy clusters and groups, extending to redshift $z \sim 2$ for massive ($M > 10^{14} M_{\odot}$) clusters, and in mass down to galaxy-sized objects at low z . More importantly, the WFXT data will be used to directly measure redshifts (from the ubiquitous Fe-K 6.7 keV line) as well as high-quality mass X-ray proxies (T, Y_X, M_{gas}) for ~ 5000 clusters, ~ 3000 of which are at $z > 0.5$, and ~ 2000 at $z > 1$ (see Fig.4). Unlike eROSITA, WFXT will resolve cluster cores out to $z > 1$, thus enabling robust measurements of X-ray mass proxies which are found to be best correlated with cluster masses when cores are excised from the data [21, 22]. Such a sample of 5000 clusters will thus be used to place constraints on cosmological models *without resorting to spectroscopic follow-up observations and other means to secure cluster redshifts and masses*. Such a cosmological sample is 50 times larger and extends to much higher redshifts than the current ROSAT-selected clusters at $z < 1$ used in cos-

mological studies of the evolution of the cluster mass function [15, 16, 17] and gas mass fraction [18]. A direct analysis of the WFXT survey data alone will provide a dramatic improvement on constraining the Dark Energy equation of state parameters, as shown in Fig.5 [19].

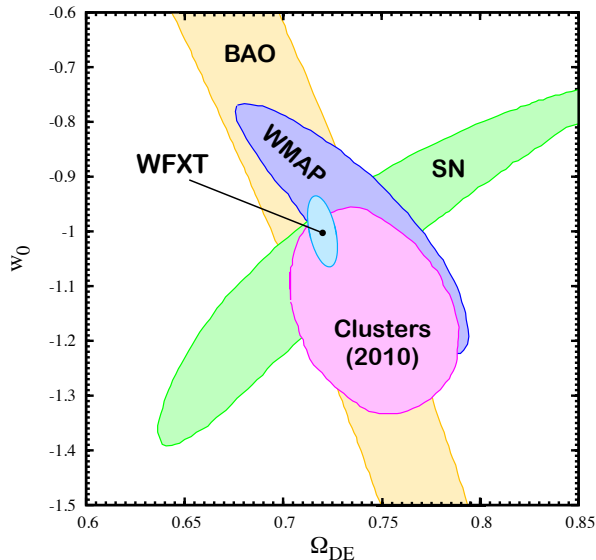


Figure 5: Constraints on the dark energy equation-of-state parameters from the Deep + Medium WFXT cluster surveys and other cosmological data sets. The latter include Baryonic Acoustic Oscillations, type-Ia SNe, WMAP and current constraints from small samples of ($\sim 10^2$) clusters based on ROSAT surveys and follow-up Chandra observations (e.g. [13]). The WFXT forecast (inner ellipse) is based on both the evolution of the cluster abundance and the power spectrum information (space distribution on large scales) of ~ 5000 clusters for which redshifts and mass proxies will be derived from the WFXT data alone [19]; w_0 and Ω_{DE} are measured with 6% and 1% accuracy (68% c.l.), when a flat Universe is assumed, with systematics well below these errors due to the precise mass calibration allowed by the internal measurement of mass proxies.

In addition, the WFXT dataset will allow us to search for deviations from the conventional Λ CDM cosmology, through the accurate measurement of the growth of structure thus complementing classical cosmological tests which probe the cosmic expansion history (e.g., BAO and SN-Ia) [20].

For example, models based on the modification of General Relativity (GR) can be tuned to provide an expansion history indistinguishable from that of Λ CDM. Still, the two models produce different histories for the linear growth of perturbations and, therefore, can be distinguished on the basis of the evolution of the cluster mass function [23]. In a similar way, deviations from Gaussian initial perturbations induce a different timing in the formation of the most massive high-redshift clusters and a distinctive signature in the scale dependence of halo bias which can be de-

tected from the large-scale cluster power spectrum based on WFXT surveys [24, 25]. Departures from Λ CDM also can be searched for by looking at the statistics and properties of the rarest objects, such as the ‘‘Bullet Cluster’’ [26] or excessively massive clusters at high- z [27]. WFXT will dramatically extend the search volume for such objects, since the Medium and Deep surveys will provide, not only detections, but also detailed X-ray images and spectra (with at least 1500 photons) for virtually every massive cluster in the surveyed lightcone to $z \sim 1.5$.

Finally, in combination with CMB anisotropy data from Planck, and with future SN-Ia and BAO probes, WFXT surveys will provide tight constraints on neutrino mass [28]. The presence of one or more species of light massive neutrinos induces a suppression of the linear growth of perturbations, due to free streaming of such particles [29]. Since this suppression is stronger on smaller scales, comparing the tight constraints on the power spectrum amplitude, provided by the cluster mass function, with that determined from CMB anisotropies has the potential to constrain (or measure) masses of one or more neutrino species with a precision better than 0.1 eV.

1.3 When and How did Supermassive Black Holes Grow?

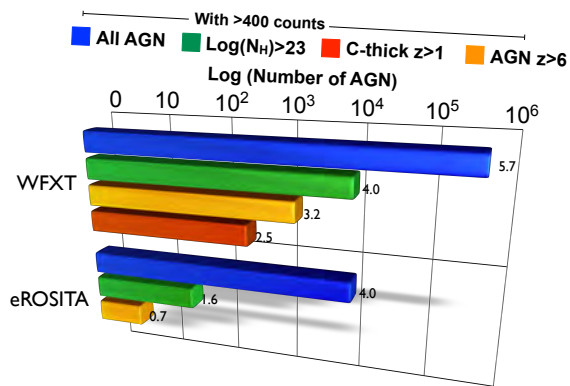


Figure 6: The AGN discovery space for (3-year long) WFXT surveys, compared with the planned eROSITA mission (2013). WFXT will detect 5×10^6 AGN overall, bars indicate the estimated numbers of AGN which will be unambiguously characterized based on their X-ray spectra with sufficiently high S/N (> 400 counts): total (blue), heavily obscured (green), and Compton-thick at $z > 1$ (red). Expected number of detected ($S/N > 3$) AGN in the early Universe are shown in orange.

The discovery that most luminous nearby galaxies host supermassive black holes (SMBHs) in their nuclei, and that SMBH masses are tightly linked to the

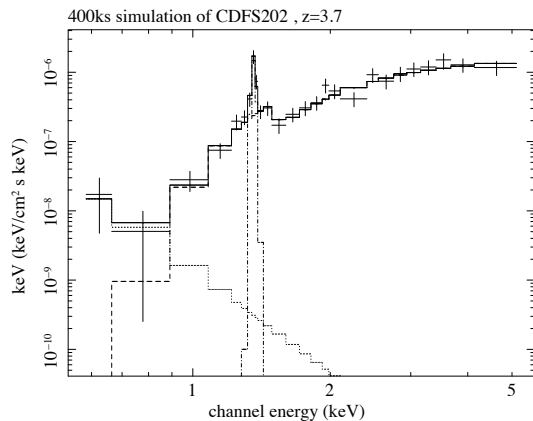


Figure 7: Simulated WFXT X-ray spectrum of a deep survey (400 ksec) obscured high redshift AGN based on the Chandra Deep Field South data for this AGN [35], $N_H = 10^{24}$, $EW_{line} = 1$ keV. There are 530 counts total. The iron line is very strong and allows an accurate redshift determination from the X-ray data alone.

structural parameters of the host spheroid [30] suggests a scenario in which SMBH feedback has a significant role in establishing and maintaining this link. It is widely agreed that the critical early growth of SMBHs is often largely obscured in the optical and UV due to gas and dust, meaning that the most efficient and reliable way of detecting cosmological populations of AGN is through X-ray observations.

X-ray surveys with Chandra and XMM-Newton have uncovered large populations of hidden AGN in both the nearby and distant Universe, but the relatively small fields of view of these observatories have limited the numbers of detected AGN. Hence, central questions about SMBH and galaxy evolution still remain unanswered: When and how did the first SMBHs form? How are nuclear activity, feedback, and star formation related to galaxy mergers, and what other processes are critical for AGN fueling? How do SMBHs grow across a wide range of large scale cosmic environments? What is the history of nuclear activity over a galaxy’s lifetime? WFXT surveys will powerfully address all these questions.

WFXT will detect a total of ~ 5 million AGN. With $\sim 1''$ positional accuracy, the vast majority of WFXT AGN will be reliably associated with multi-wavelength counterparts, using data from wide-area optical, infrared, and radio surveys, *e.g.*, Pan-STARRS, VISTA, EVLA, ASKAP-EMU, MeerKAT, LSST, Euclid, WFIRST, and SKA [31, 32]. Prompt identification enables efficient large-scale spectroscopic and multi-wavelength source characterization, especially important for the generally faint sources

at high redshift ($z > 1.5$). WFXT will provide good-quality X-ray spectra (> 400 photons) for $\sim 5 \times 10^5$ AGN, including 10^4 heavily obscured objects ($\log N_H > 23$) as well as a few hundred Compton-thick AGN in the distant Universe ($z > 1$), a task which is beyond eROSITA’s capabilities (see Fig.6). An example is shown in Fig.7, where a simulated WFXT spectrum of the Compton-thick AGN CDFS-202 at $z = 3.7$ [34, 35] is displayed (400ks integration, returning 530 photons).

WFXT will produce an unrivaled sample to study the evolution history of obscuration (*e.g.* relation with z and L_X), covering factor, iron lines, etc. [33]. There will be about 10^4 WFXT AGN observed with more than 10^4 counts, which will allow unprecedented study of BH physics of a large AGN population. WFXT will provide the first large (about 1200–9000 objects) and reliably identified sample of obscured and unobscured AGN at $z > 6$, and it should detect tens of AGN even at $z = 8–10$ [36]. These high-redshift, moderate-luminosity AGN will allow a direct and unbiased study of typical growing SMBHs through the era of reionization and into the cosmic dark ages. Currently, the space density of such $z > 6$ AGNs is uncertain by at least a factor of 20. The large number of $z > 6$ AGN detected by WFXT will fully populate the luminosity-redshift space as needed to constrain models for early SMBH growth. For comparison, only about 30 AGN at $z > 6$ are known today, and these are luminous and unobscured quasars (spectacular but rare) owing to optical selection bias.

WFXT observations will provide the most efficient, reliable means of finding and characterizing SMBH accretion within the billions of galaxies detected by the next generation of wide-field optical, infrared, and radio surveys. Moderate to heavy levels of nuclear obscuration and various degrees of optical/UV dilution by host galaxy starlight are expected for about half the ~ 5 million AGN that will be reliably identified by WFXT. Without WFXT, it would be difficult even to find, let alone characterize, this large fraction of AGN, even with very high-quality data at other wavelengths, and neglecting them would lead to an incomplete, biased AGN sample.

Recent studies have begun to explore the connection between AGN activity and host large-scale structures, and with more accurate measurements we can start to distinguish between models of black hole fueling and evolution. However this requires accurate clustering measurements, and thus wide (> 10 deg²) contiguous fields and large AGN populations with secure multi-wavelength counterparts, which will only be possible with a sensitive wide-field X-ray mission.

The enormous and highly complete WFXT AGN

sample will enable the definitive study of SMBH growth from $z = 0.1$ to 6 for the full range of galaxy types and across the broadest span of cosmic environments, ranging from superclusters to voids. The sample will be sufficient to determine the distribution of SMBH growth rates in multiple bins of large scale environment, host galaxy mass and star formation rate, merger activity, and redshift while still retaining excellent source statistics (typically 500-1000 AGN or more) in essentially all bins.

1.4 Time Domain Studies

The unique capabilities of WFXT in terms of effective area and field of view make it suitable for conducting timing studies for an unprecedented number of moderate and high redshift AGNs, and to discover and constrain rates and properties of distant, faint and rare variable X-ray populations. Simulations show[37] that the core WFXT surveys will allow us to discover hundred of transient and variable X-ray sources. The ten 40 ksec epochs of the WFXT deep surveys will provide outstanding time domain information on AGN, effectively sampling the full range of AGN parameter space (e.g., luminosity, redshift, and Eddington fraction) across a broad part of the variability power spectral density function.

The WFXT deep surveys will be sited on well-studied sky areas that will have highly complementary optical and infrared variability data across hundreds of time intervals (e.g., the LSST Deep Drilling Fields). The combined data set will allow characterization of coordinated multi-band AGN variability as a function of SMBH accretion properties, as well as studies of remarkable transient AGN activity (e.g., accretion disk instabilities, absorption variation events, jet flares, and stellar tidal disruptions). Additional GO observing programs (e.g. Galactic Center and local galaxy observations) will greatly expand the WFXT time domain science. WFXT will be an ideal and unique facility to validate and characterize astronomical events detected by future Gravitational Wave and Neutrino experiments (e.g., [38]) which will have positional uncertainties of a few deg².

2 Mission Concept and Preliminary Design

The science payload consists of three separate, but identical, X-ray telescope/detector modules as illustrated in Fig.8. These units mount to a simple spacecraft that provides the usual complement of services (i.e., power, command and data handling, telemetry,

attitude control, etc.). This configuration provides clean interfaces between the science payload and the spacecraft to minimize complexity and reduce overall costs. The derived performance requirements for the WFXT science instrument and spacecraft systems are summarized in Tables 2 and 3.

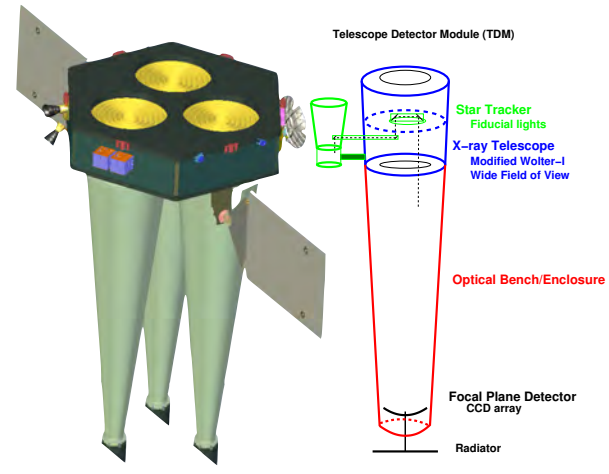


Figure 8: The WFXT Science Payload consists of three telescope/detector. The telescopes are modified Wolter-I, designed to provide a 1 degree field of view with $\sim 5''$ HEW angular resolution averaged across the field. The focal plane consists of a 2×2 array of CCDs similar to those operating on Chandra and Suzaku. Low power hybrid electronics are used to readout the CCDs, which are passively cooled to -120°C . A star tracker is included with each telescope to provide information for reconstruction of images similar to previous X-ray astronomy missions such as Chandra. The telescopes and detectors are enclosed in an optical bench structure to maintain alignment and to shield against stray light and out of band radiation.

Table 2: WFXT Mission Performance Requirements

Parameter	Requirement	Goal
Area (1 keV) ^(*)	$7,000 \text{ cm}^2$	$10,000 \text{ cm}^2$
Area (4 keV)	$2,000 \text{ cm}^2$	$4,000 \text{ cm}^2$
Field of View	$1^\circ \times 1^\circ$	$1^\circ \times 1^\circ$
Angular Resolution (1 keV)	$5''$ HEW	$\leq 5''$ HEW
Pixel Size	$\sim 1''$	$\sim 1''$
Energy Band	0.2 - 4 keV	0.1 - 6 keV
Energy Resolution	$\frac{E}{\Delta E} > 10$	$\frac{E}{\Delta E} > 20$
Time Resolution	< 3 seconds	< 1 second

(*) The WFXT $\sim 0.7 \text{ m}^2$ area meets that required in our earlier Astro2010 mission concept, but is $\sim 2/3$ of the goal.

WFXT operates in a pointed mode with the core surveys built up through a series of observations. The medium survey consists of a mosaic of individual 13 ksec/deg² pointings covering the desired area. The deep surveys consist of similar mosaics in repeated 40 ksec/deg² observations spaced over the mission to allow for time domain studies. Most Guest Observer observations are expected to be single point-

Table 3: WFXT System Requirements

Parameter	System Requirement
Orbit	10,000 x 140,000 km 28.5° inc.
Mission Lifetime	5 years
Payload Mass	1600 kg (CBE)
Module Envelope	7 m length, 1.3 m diameter
Payload Power	375 W (CBE)
Target Acquisition	1'
Pointing Stability	2'' per 2-3 seconds
Pointing Knowledge	1-2''
Slew Rate	0.3 deg/sec

ings. However, GO surveys will be supported and carried out in similar fashion to the core surveys. WFXT will be launched using either an Atlas V 431 EEVL or Falcon 9 ELV from the Kennedy Space Center (KSC) and placed in highly elliptical orbit (HEO) similar to the Chandra X-ray Observatory orbit. For this RFI we use the Atlas V 431.

2.1 Science Payload

The telescope/detector modules each consist of a wide-field X-ray telescope, optical bench, fine attitude sensor, and X-ray detector assembly. The X-ray telescopes are nested shells based on a polynomial perturbation of the classical Wolter-I prescription [39]. The wide-field design has been successfully built and tested [40] using an epoxy replica on a silicon carbide (SiC) mirror shell. The long time gap since that demonstration shell was fabricated has allowed the team to develop a different approach for manufacturing the WFXT shells. This effort has been ongoing at INAF-Osservatorio Astronomico di Brera (see Appendix A for details), funded through Agenzia Spaziale Italiana (ASI) and Istituto Nazionale di Astrofisica (INAF). A prototype mirror is currently under construction using thin fused silica [41], and direct grinding and polishing to achieve the desired figure and smoothness. It is scheduled for X-ray testing at the Panter facility in late November of this year. Fig.9 shows the new shell in the final figuring and polishing machine, and Fig.10 shows the predicted HEW performance of this shell as well as the measured performance of the earlier SiC shell. Appendix A describes the mirror technology development plan that will take the mirrors from TRL 4 to TRL 5 based on X-ray measurements of the prototype shell this calendar year (2011). We include fabrication of a telescope engineering model during Phase A to advance the TRL from 5 to 6 prior to Phase B start. All other science components, including the detectors, are al-

ready at TRL 6 or higher.



Figure 9: Prototype of a wide-field X-ray telescope fused silica shell, 50 cm in diameter, 20 cm long and 2 mm thick, in the final figuring and polishing machine. The shells are manufactured by Heraeus and ground to a conic approximation. Out of roundness corrections are made using a precision lathe prior to the final polishing and figuring.

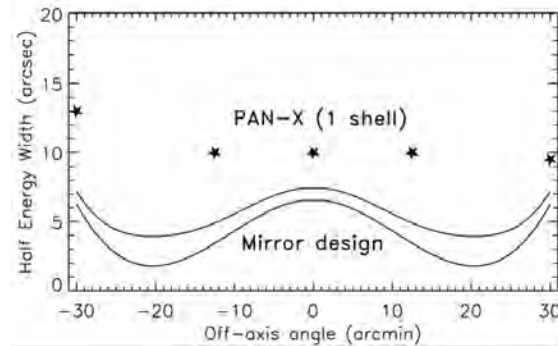


Figure 10: HEW versus Off-axis angle. The lower solid curve is the design performance for WFXT (a field average HEW of $\sim 3.5''$). The slightly higher solid curve is the performance expected including the effects of a $3.5''$ manufacturing error, the field average HEW is $\sim 5''$. The stars are measurements from the SiC (Pan-X) prototype and represent achieved technology.

The detectors are 2×2 arrays of X-ray CCDs. The baseline device is an MIT/ Lincoln Laboratory CCD similar to those in operation on Chandra (launched in 1999) and Suzaku (launched in 2005). These are frame transfer devices, with low noise (2-3 electrons rms) performance resulting in Fano limited energy resolution over the WFXT bandwidth. The CCD operating temperature is -120°C . As with Chandra, each array of CCDs is passively cooled via a $\sim 0.25 \text{ m}^2$ radiator, and trim heaters are used to adjust the temperature as needed. The CCDs are read out every 3 seconds and X-ray events are identified using

dedicated front end signal processors to record position, amplitude and frame time for transmission to the ground and post-facto image reconstruction. The CCDs have thin aluminized optical blocking filters to protect against scattered light similar in design to those used on both Chandra and Suzaku. Based on Chandra experience, there is a two position filter wheel in front of each CCD array. The closed position shields the CCDs from low energy protons during perigee passage through the Earth's radiation belt and from solar storms, eliminating this cause for CTE degradation.

Each telescope includes a star tracker that provides the ≤ 2 arc second pointing information needed to accurately locate the X-ray events on the sky. This is similar to systems used on Chandra and XMM-Newton. The star tracker will include a fiducial light system to monitor the X-ray CCD location relative to the line of sight of the X-ray telescope. The use of individual fine attitude systems for each telescope module greatly reduces the requirements on mechanical alignment tolerance and stability of the three telescope modules, thereby simplifying the overall mission design and reducing total cost. The WFXT star tracker precision requirement is an order of magnitude less demanding than the Chandra tracker. Standard commercially available star trackers meeting the WFXT requirements will be selected from several candidates during the preliminary design study.

2.2 Spacecraft

Existing, reliable spacecraft architectures, materials and methods will be employed to support the instrument and achieve the mission goals while minimizing cost. For example, for this RFI we use a generic spacecraft with a Chandra-like configuration including dual string redundancy to fulfill a 5 year mission lifetime. A standard mono-propellant hydrazine propulsion system is used for momentum management, i.e., reaction wheel dumps. No new developments are needed to meet the WFXT requirements.

The spacecraft accommodates the three X-ray telescope/detector modules with the telescope ends embedded into the bus, which minimizes the center of gravity height in the launch vehicle. The spacecraft fits into the Atlas V 4-meter standard Long Payload Fairing as illustrated in (Fig.11) showing the overall dimensions of the stowed and deployed spacecraft.

The spacecraft is a 3-axis stabilized zero momentum system. S/C mounted star trackers provide attitude data, a space inertial reference unit (SIRU) provides rate data, Sun sensors provide the Sun direction in safe mode. Four reaction wheels in a pyramid configuration are used for pointing. The spacecraft can

roll about the payload boresight prior to the start of target observations to place the solar arrays in optimal orientation to the Sun. The spacecraft slews for communications and data dumps scheduled during perigee pass when observations are suspended due to the Earth's radiation belt.

Spacecraft power is a 28V system with two deployable solar arrays and one 60 A-hr Lithium-Ion battery. The 6.4 m² arrays provide 2,000 W of power at end of life. A standard 1553 data bus is used for the spacecraft and instrument commands/telemetry. A RAD750 processor is used for processing and storage of commands, telemetry, and data. The anticipated data rate is ≤ 128 kbps (science and engineering data), and the 128 Gbit memory is able to hold 10 days of data providing ample reserve if a download is missed. The observing program will be uploaded weekly, and executed autonomously similar to the operating mode on Chandra. WFXT will use the Deep Space Network (DSN) for communications. Data dumps will be scheduled during perigee passes (approximately every three days). Additional contacts will be used to monitor health and safety. These passes provide the necessary tracking for updating the WFXT orbital elements and ephemeris. X-band communications are baselined and provide adequate bandwidth for the mission. However, alternates such as S or Ka band will be investigated.

The system level mass and power budgets for the observatory are shown in Table 4. The total observatory (flight system) launch mass (with propellant and 26% overall contingency) is 2697 kg. The Atlas V 431 launch vehicle is capable of lifting > 3500 kg to the desired orbit, providing a total unallocated mass margin of $> 30\%$. The total power requirement with 22% overall contingency is 1116 W, and the end of life observatory power available is 2,000 W providing an unallocated power margin of 79%.

3 Organization and Management Approach

WFXT combines the talents and processes of JHU/Homewood and JHU/APL, MSFC, INAF (Italy) and MIT/LL. The mission is led by the PI Dr. Stephen S. Murray (JHU), an experienced astrophysicist with the scientific, technical and management experience to fulfill this role (Fig.12). Deputy PI Dr. Piero Rosati (ESO) and PS Dr. Andrew Ptak (GSFC) bring additional scientific expertise and extensive data processing experience to the mission. Nobel-prize recipient Dr. Riccardo Giacconi (JHU) is the Senior Science Adviser, and the Science team

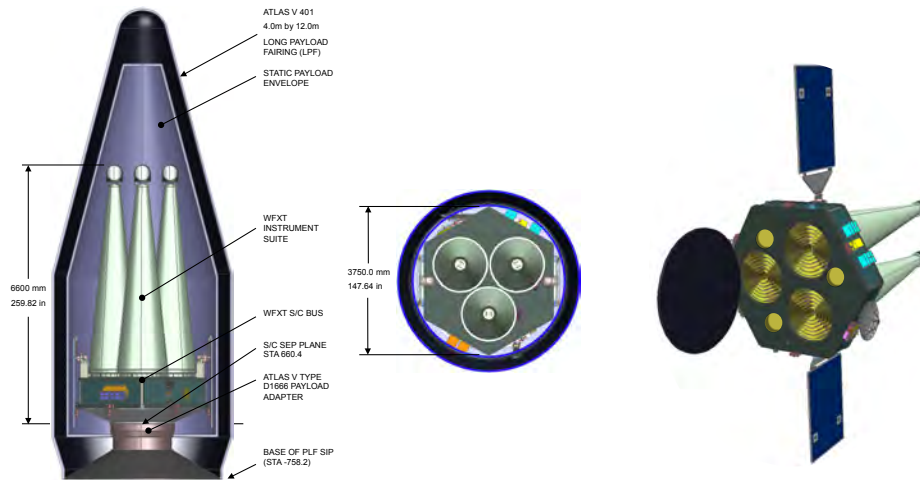


Figure 11: Two views of WFXT in the stowed configuration (left) fitting within the Atlas V fairing, and WFXT in the deployed configuration (right)

Table 4: Mass and Power Budget - Current best estimates (CBE) and contingency (Cont) are listed by subsystem. Margins of 30% for mass and 79% for power are in addition to contingencies of 26% and 22%.

Item/Subsystem	Mass			Power		
	CBE (kg)	Cont. (%)	Total (kg)	CBE (W)	Cont. (%)	Total (W)
Structures & Mechanisms	405	20	486			
Electrical Power & Distribution	118	32	156	29	27	34
Command & Data Handling	60	15	69	105	5	110
Telecom	35	11	39	43	7	46
Thermal Control	30	25	38	71	25	89
Attitude Determination & Control	71	6	75	100	5.0	105
Payload Adaptor	100	20	120			
Propulsion - dry	25	7	27	60	15	69
S/C Bus - dry Total	844	20	1010	408	11	453
Telescope & Structure	900	30	1170	225	30	292
Optical Bench	225	20	270	75	30	97
CCD Camera and Electronics	75	30	98	135	30	176
Star Tracker/Fiducial Lights	60	30	78	75	30	98
Science Payload Total	1260	30	1638	510	30	663
Flight System - dry	2104	26	2648	918	22	1116
Propellant			49			
Flight System - launch			2697			1116
ELV Capacity to Orbit		Atlas V 431	3500	EOL Observatory Power		2000
Mass Margin (kg)			803	Power Margin (W)		884
Mass Margin (%)			30	Power Margin (%)		79

Table 5: Bottoms Up Cost Estimate \$779M (FY12 dollars) including GO program and reserves, and exclusive of launch services (estimated range \$90–180M)

PM/QA MSE	Science Pre-launch	Science Instr	S/C BUS	Ground System	I&T LEOP	EPO	Mission Ops	Reserves [†]	GO Grants	Total
70	5	195	140	50	55	10	60	169	25	779

[†] 30% reserves Phase A,B,C/D = \$156M, 20% reserves Phase E = \$13M (exclusive of GO grants)

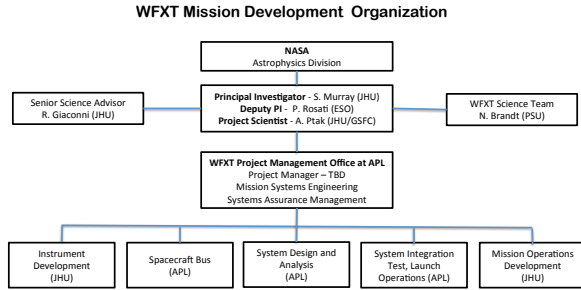


Figure 12: The WFXT Development Organization is managed at APL as shown in this chart. The major areas of responsibility and the subsystems associated with these are indicated. There are clear and unambiguous lines of authority and responsibility to assure a successful mission.

is led jointly by Drs. Niel. Brandt (PSU) and Piero Rosati. MSFC is responsible for the ground calibration and integration of the telescope/detector modules. Project management, system engineering and quality assurance are led by APL, which has considerable experience in formulating and implementing end-to-end missions of this class for NASA.

4 Schedule

The WFXT 66 month development and 60 month science operation schedule is shown in Fig.13. PDR is approximately 13 months from the Phase B start, with the CDR about 5 months after the start of Phase C. The extended Phase A allows the fabrication of an engineering model to advance the mirror TRL level and validate the shell holding fixture design. An early telescope PDR and CDR 6 months later will allow an early start of flight model fabrication. Similarly, the CCD procurement from MIT/Lincoln Labs has a long lead time, and the extended Phase A includes an early start to minimize schedule risk and assure that the CCD's are available for integration with the flight telescopes for end-to-end calibration at the MSFC X-ray Calibration Facility (XRCF).

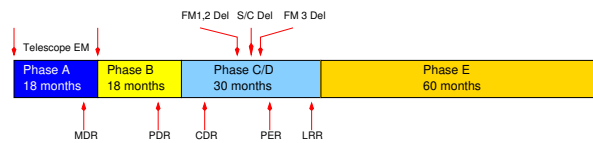


Figure 13: WFXT schedule - 66 month development (Phase A, B, C/D) and 60 month mission operation (Phase E). Major milestones and reviews are shown.

5 Cost

The estimated total life cycle mission cost for the WFXT mission is \$779M (FY12 dollars), including reserves and GO grants, but exclusive of launch

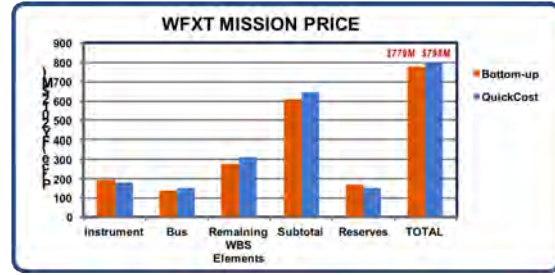


Figure 14: Independent Cost Estimate using QuickCost

services. This estimate includes 30% reserves for Phases A,B and C/D (\$156M) and 20% for Phase E (\$13M).Table 5 summarizes this cost estimate by mission elements. WFXT is compatible with either an Atlas V 431 (\$180M) or a Falcon 9 (\$90M).

Costs were developed using a bottom-up estimate performed by the WFXT institutions: INAF/Brera for the telescopes and MIT/Lincoln Labs for the detectors; and estimates from potential contractors. Some costs were estimated by analogy with Chandra, others are based on commercial procurement. The spacecraft costs were developed by analogy with the Chandra bus as well as ROM estimates from aerospace industrial sources. The Phase A, Phase E and the EPO costs are taken from FUSE and Chandra analogy, and the GO grants set at ~ \$5M per year.

To enhance our cost credibility, an Independent Cost Estimate (ICE) was performed. The QuickCost model, developed by Dr. J. Hamaker for NASA, was used.¹ A conservative approach was used to select model inputs. E.g., the instrument complexity and the instrument % New Design were both entered as 100%. Phase A studies, Mission Operations and GO grants were not estimated using QuickCost; bottom-up data were used as throughput values for these WBS elements. Launch services were not included in bottom-up or QuickCost estimates. WBS allocation percentages calculated in the QuickCost Satellite model were used to derive WBS element prices in the QuickCost Satellite Trades model. The results of the ICE (\$FY12) are shown in Fig.14. Costs are shown at a risk probability of 50% prior to the addition of reserves. The QuickCost estimate with reserves, at a probability of 70%, is \$798M (and includes the Phase A, Mission Operations and GO grants). This indicates that the bottom-up estimate with reserves, \$779M, is credible at this early pre-study phase.

¹Other cost models such as NICM were considered, but not used because WFXT mass and power did not fit within the range of either the particle or optical sensor databases. See Appendix B for details.

References

- [1] New Worlds, New Horizons in Astronomy and Astrophysics, National Academies Press 2010
- [2] Murray, S. S., et al., 2008, SPIE Proc, 7011
- [3] WFXT Web Site, <http://wfxt.pha.jhu.edu>
- [4] Giacconi, R. et al. 2009, Astro2010 Science White Paper, astro-ph/0902.4857
- [5] Vikhlinin, A. et al. 2009, Astro2010 Science White Paper, astro-ph/0903.5320
- [6] Murray, S. et al. 2009, Astro2010 Science White Paper, astro-ph/0903.5272
- [7] Ptak, A. et al. 2009, Astro2010 Science White Paper, astro-ph/0902.4239
- [8] Elvis, M. et al. 2009, ApJS, 184, 158
- [9] Madrid, J. P. and Macchetto, F. D., 2009, astro-ph/0901.4552
- [10] Rosati, P. et al., 2002, ARA&A, 40, 539-577
- [11] Voit, G. M., 2005, Reviews of Modern Physics, 77, 207-258
- [12] eROSITA Mission Definition Document, <http://www.mpe.mpg.de/erosita/MDD-6.pdf>
- [13] Vikhlinin, A., et al. 2009, ApJ, 692, 1060
- [14] Rosati, P. et al., 2002, ARA&A, 40, 539-577
- [15] Vikhlinin, A. et al., 2008, arXiv:0812.2720
- [16] Borgani, S. et al., 2001, ApJ, 561, 13
- [17] Allen, S. W., Evrard, A. E., & Mantz, A. B. 2011, ARAA, 49, 409
- [18] Allen, S., et al., 2008, MNRAS, 383, 879
- [19] Sartoris, B. et al. 2011, MNRAS, submitted
- [20] Albrecht, A. et al., 2006, Dark Energy Task Force Report, arXiv:astro-ph/0609591
- [21] Kravtsov, A.V. et al. 2006, ApJ, 650, 128
- [22] Pratt, G. et al. 2009, A&A, 498, 361
- [23] Schmidt, F., Vikhlinin, A., & Hu, W. 2009, PhRD, 80, 083505
- [24] Dalal, N. et al., 2008, Physical Review D, 77, no. 12, 123514
- [25] Sartoris, B. et al. 2010, MNRAS, 407, 2339
- [26] Farrar, G. R. & Rosen, R. A., 2007, Physical Review Letters, 98, no. 17, 171302
- [27] Mortonson, M.J. et al. 2011, Phys.Rev. D, 83, 023015
- [28] Mantz, A., Allen, S. W., & Rapetti, D. 2010, MNRAS, 406, 1805
- [29] Hannestad, S. 2010, Progress in Particle and Nuclear Physics, 65, 185
- [30] Gebhardt, K., et al., 2000, ApJ, 539, L13
- [31] Luo et al., 2010, ApJS, 187, 560
- [32] Brusa et al., 2011, Mem S A It Supp, 17, 106
- [33] Matt and Bianchi, proceedings of the WFXT Bologna meeting
- [34] Norman, C. et al., 2002, ApJ 571, 218
- [35] Comastri, A. et al., 2011, A&A, 526, L9
- [36] Gilli, R. et al. 2011, Mem SAI Supp, 17, 85 (Procs. of the Bologna WFXT Workshop, 2009)
- [37] Paolillo, M. et al., 2011, Mem S A It Supp, 17, 97 (Procs. of the Bologna WFXT Workshop, 2009)
- [38] Guetta, D. & Eichler D., 2010, ApJ, 712, 392
- [39] Burrows, C. J., Burg, R., & Giacconi, R. 1992, ApJ, 392, 760
- [40] Ghigo, M. et al., 1999, Proc SPIE Vol 3766, 207
- [41] Citterio et al., 2011, SPIE Proc, 8147
- [42] Conconi, P., & Campana, S. 2001, A&A, 372, 1088
- [43] Conconi, P. et al., 2010, MNRAS, 405, 877
- [44] Citterio, O., et al., 1999, Proc. SPIE Vol. 3766, 198
- [45] Choo, T. H. et al., 2008, AIAA SPACE 2008 Conf, 7656

A Technology Development

X-ray optics with high resolution across a wide field of view have been designed and demonstrated using a modified Wolter-1 prescription based on a polynomial perturbation as described by Burrows, and Giacconi [39] and later refined by Conconi and Campana [42, 43]. The most recent prototype was produced by Citterio et al. [40, 44] in the late 1990’s using a SiC shell and epoxy replication, achieving the desired 10 arc second HEW across a 1 degree field of view. Since that time a new manufacturing process has been adopted to improve the performance to 5 arc seconds HEW (averaged over the field of view). This new process uses direct figuring and polishing of thin mirror shells made from fused silica following initial raw grinding to an approximate figure. The approach is similar to that used to manufacture the Einstein, ROSAT and Chandra mirrors, but applied to much thinner shells. The process is enabled by new manufacturing processes and machinery as described below. Extensive finite element model analysis has shown that the mirror performance is dominated by the shell profile and that suitable holding and integration processes do not add significantly to the resolution error budget. Hence the critical development effort is in manufacturing the individual shells to the required figure and surface smoothness. A prototype mirror shell based on this new process is well underway, with X-ray testing scheduled for the end of November, 2011.

A.1 Material Choice

The monolithic mirror shell material must meet a variety of requirements, not all of equal importance. A light, yet stiff material with good thermo-mechanical properties is needed. Furthermore the material must be machinable to very high precision so that it can be correctly figured. And finally it must be capable of being polished to a surface roughness of a few nano-meters. Fused silica is a well known material that is used for precision optics in both ground and space applications. It is low density ($\rho = 2.203 \text{ gm cm}^{-3}$), has a low coefficient of thermal expansion ($0.5 \times 10^{-6} \text{ K}^{-1}$), and a good modulus of elasticity (70 GPa). Fused silica is also attractive because of its low cost and timely availability. A drawback related to fused silica is that it is brittle and suffers surface damage during grinding. However, these issues can be overcome with suitable chemical etching and extended polishing as demonstrated in the past use of fused silica (or other glass material) for high resolution X-ray optics. The critical challenge is

Table 6: Prototype Mirror Parameters

Parameter	Value
Focal Length	5500 mm
Diameter at Intersection Plane	487 mm
Thickness	2 mm
Total Length	200 mm
Material	Fused Silica
Profile	Polynomial

to obtain both high angular resolution and low surface scattering over a large field of view while keeping the shell relatively thin with respect to previous glass shells.

A.2 Manufacturing Process

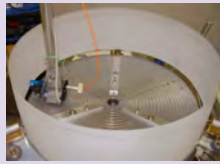
The production flow for the WFXT mirrors is illustrated in Fig.15. The process starts with a fused silica glass tube that is an available commercial product. The tube is rough figured with a double cone profile and a thickness of a few millimeters. The raw fused silica tube for the prototype mirror, and the first grinding were provided by Heraeus Quarzglas GmbH and Co. KG (Germany). The shell is then characterized in terms of its out-of-roundness (OOR) errors after supporting it in an astatic support jig for metrology. Shells that meet the initial OOR requirement are integrated into a shell support structure (SSS) that holds the shell through the remaining process steps, allowing the necessary machining and metrology and other steps to be carried out before the shell is assembled into the telescope structure.

With the shell mounted to the SSS, the next step is to correct the OOR errors with a fine grinding process. This step is carried out on a high precision lathe (e.g. one provided by LT Ultra Precision Technology GmbH), with grinding wheels and a metrology system that are mounted directly on the lathe.

When the OOR errors are reduced to acceptable levels, the shell is figured and polished to the final profile using a “deterministic” figuring method. This technique transforms measurements of the current shell profile to a correction matrix that is used to drive a computer numerically controlled (CNC) polishing machine whose material removal rate is well calibrated. A Zeeko IRP600 machine developed by the Zeeko Company (based in Great Britain) is used. The Zeeko is a seven axis CNC machine that uses an innovative figuring and polishing approach and a patented tool to provide a distributed pressure and variable area head for the polishing of aspheric and complex forms.



Raw grinding. Starting from a raw Fused Silica glass tube, first grinding operations are performed to obtain a double cone profile at the required thickness of a few millimeters.



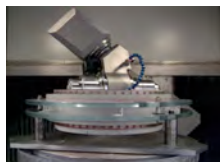
Out-Of-Roundness Metrology. The shell is characterized in terms of Out-Of-Roundness errors, supporting it onto an astatic support jig.



Temporary stiffening. The shell is integrated into a special “Shell Support Structure”, a suitable jig structure able to allow the metrology, machining and all the necessary operations before the assembling of the shell into the final structure.



Fine grinding. An Out-of-Roundness correction is obtained by means of a fine grinding process. These operations are performed using a high precision lathe and with a proper metrology system mounted on the machine.



Polishing. The polishing process is performed by CNC polishing systems, controlled on 7-axis, that use a patented tool to provide a distributed pressure and variable area head for the polishing of aspheric and complex forms. The tool used for polishing is also called “Bonnet” and it is given by a spinning, inflated, membrane-tool compressed against the surface of the mirror.



Superpolishing. A superpolishing process is performed by means of a pitch tool mounted onto the Zeeko CNC machine, in order to remove the remaining mid-frequencies errors left by the Bonnet polishing and to achieve the required micro-roughness.

Figure 15

In the Zeeko-Classic process, also called “Bonnet polishing”, a spinning, inflated, membrane-tool is compressed against the surface of the part to be machined, creating an area of contact that defines the removal footprint. It should be noted that before starting the real “figuring” process to obtain the desired longitudinal profile, a constant thickness polishing for surface damage removal is performed. Once the desired profile is obtained by means of figuring and polishing, a superpolishing process is performed using a pitch tool mounted on the Zeeko CNC machine that removes residual mid-frequency errors left by the Bonnet polishing.

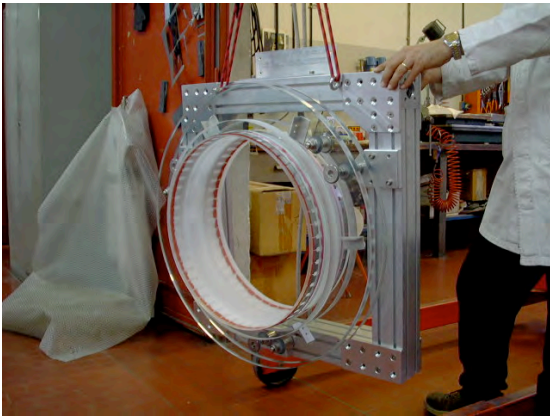


Figure 16: Fused silica shell in support structure used for figure and polishing on the Zeeko CNC machine.

A.3 Current Status

At the time of this RFI (October, 2011) a mirror shell (Fig.16) with the parameters listed in Table 6 is almost completed. Figs.17 and 18 show the predicted HEW performance of the two reflecting surfaces as a function of the off-axis angle based on the measured profiles. The front surface is complete and almost perfectly matches the design performance, while the rear surface is still in process and has not yet converged to the final profile. A final superpolishing step is underway to remove residual high frequency slope errors prior to the X-ray calibration at Panter/MPE scheduled for the last week of November 2011.

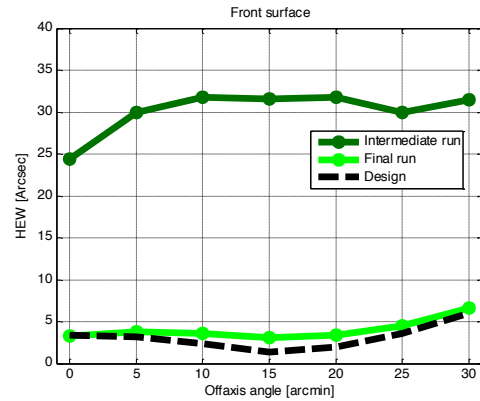


Figure 17: The calculated HEW vs. off-axis angle for the front surface of the prototype fused silica mirror. The final super-polishing run is in very close agreement with the design performance.

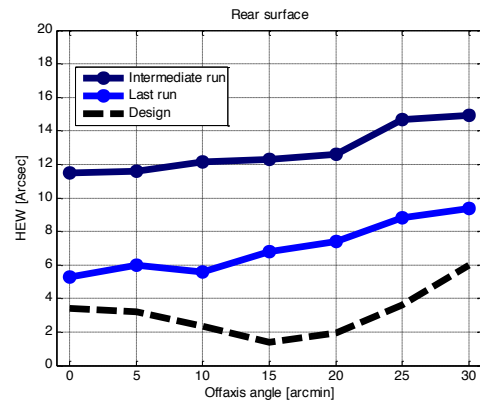


Figure 18: The calculated HEW vs. off-axis angle for the rear surface of the prototype fused silica mirror. The last run shows deviations from the design which are residuals from the Bonnet polishing that have not yet been reduced through the super-polishing process.

B Cost Estimate

B.1 Bottom-Up Cost Estimate

The bottom-up cost by Phase is shown in Table 7. The project implementation costs were developed by the Johns Hopkins University, Applied Physics Laboratory. Costs for WFXT project management, system engineering, mission assurance, instrument accommodation, observatory integration and test, and launch operations, were developed using recent data from the NewHorizons, MESSENGER, STEREO, and FUSE missions. The spacecraft bus is assumed to be procured from industry as a commodity item; several companies, have an existing bus design that will meet WFXT needs, and for the purpose of this RFI we have used an average of these estimates. During further mission studies, APL may choose to consider an in-house spacecraft build, provided that approach offers significant cost savings and risk reduction.

The instrument costs, including technology development, were developed by JHU and the instrument development team. Telescope shells were priced by INAF/Brera. The instrument Phase A costs allow for a telescope engineering model. A significant funding margin was applied (50%) to mitigate risks associated with this critical flight element. The result is an allocation of \$90M (before reserve) to develop and fabricate the three flight telescopes. It is possible that the Italian government will fund part, or all, of the telescope optics, but at this point no commitment has been formally requested or offered.

The other portions of the instrument are better understood and easier to cost. The CCD camera estimates come from MIT/Lincoln Labs, and are based on analogous designs from Suzaku. The estimate includes the design, fabrication, and testing of 36 CCD detectors (12 are required for flight). The estimate also includes packaging and thermal design, analog and digital electronics, testing, and calibration. The rolled up cost for three assembled cameras is \$60M (before applying 30% reserve).

There are additional items that are also costed to complete the building and testing of three telescope assemblies: three optical benches and close-out (\$20M); three star trackers (\$3M); fiducial light system (\$2M); three instrument integrations (\$10M); three instrument calibrations (\$5M). These additional items rollup to \$40M (before 30% reserve). Instrument costs after integration into the observatory are carried by the system integration and test (I&T), and launch and early operations budgets (LEOP). These instrument elements rollup to a total of \$190M (before reserve). Project reserves (30%) were applied

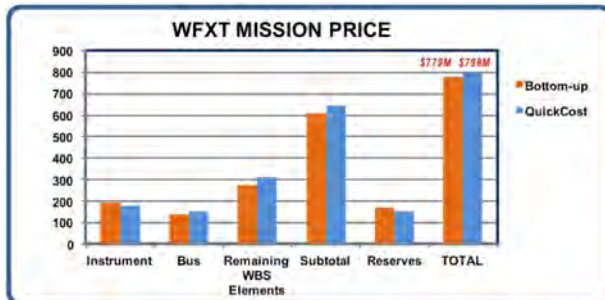


Figure 19: WFXT Mission Price

to all pre-launch mission elements.

The \$65M (plus \$13M reserve) cost estimate for the Phase E mission operations was developed using historical data from FUSE and STEREO, and by analogy with Einstein, ROSAT and Chandra X-ray missions, and includes \$5M for EPO. Much of the mission operations is similar to Chandra, and because we do not anticipate targets of opportunity (ToO) much can be automated. The generation of pointing schedules will be performed using either of both of the Chandra modified SPIKE (from STScI), or APL SciBox [45] which has proven to be effective in the generation of highly accurate instrument pointing scripts on MESSENGER and CRISM. Mission operations staff will consist of a team of 12–15 full time equivalents. Science operations staff will also number 12–15 full time equivalents.

B.2 Independent Cost Estimate (ICE)

B.2.1 Mission and Individual WBS Element Model

The NASA QuickCost 5.0 model developed by Dr. J. Hamaker was used for the WFXT Independent Cost Estimate (ICE). QuickCost uses statistically validated cost estimating relationships (CERs) and schedule estimating relationships (SERs) to estimate satellite costs. Using a database of 131 missions, it can estimate spacecraft, instrument, and other typical NASA mission WBS elements. QuickCost provides prediction intervals on cost estimates allowing the user to specify a desired level of confidence. An example is shown in Table 8. The QuickCost Satellite Trades tool was used to determine the WFXT life cycle cost estimate; however, Satellite Trades does not calculate individual WBS element costs to compare with the bottom-up estimate, only the QuickCost Satellite tool allocates individual WBS element costs. The Satellite tool was used to determine the in-

Table 7: Bottom-Up Cost Estimate

Description	ØA	ØB	ØC/D	ØE	Total Mission Costs (\$FY12)
	18 months	18 months	30 months	60 months	
PM/MSE/QA	15	20	35		70
Science (Pre-launch)	1	1	3		5
Instrument (Design, Fab, Cal)	5	70	120		195
Spacecraft Bus		25	115		140
Ground Systems		10	40		50
I&T and Launch and Early Operations			55		55
EPO		2	3		5
Reserves (30%)*	6	38	112		156
Pre-launch Total (A/B/C/D)	27	166	483		676
Mission Operations (Phase E)				60	60
EPO				5	5
Phase E Reserves (20%)				13	13
Operations Phase Total				78	78
Guest Observer grants				25	25
Mission Total	27	166	483	103	779

Table 8: QuickCost Reserve Calculation at 70%

Variable	Make Inputs in Blue Cells	Variable Units
Median Estimated Cost (millions of dollars)	\$902.0	DOT&E + TFU (Phases B/C/D) in Millions Dollars including fee, including full cost for full cost years (excluding ground system, launch services and MO&DA—which are all calculated below)
Desired Confidence Level (percentile)	70%	Enter desired confidence level (in the cell to the left).
Median Cost + Reserve to Achieve Desired Confidence Level	\$620.0	Note: This confidence level accounts for the Prediction Interval of the CER only and assumes this dominates uncertainties in the input variables.

Table 9: QuickCost Satellite Tool Input Table with WFXT Data

Variable	Make inputs in Blue Cells	Variable Units
Destination (earth orbital or planetary)	1.0	0 = earth orbital or 1 = planetary
ATP Date Year Month Year	2016	Authority to Proceed date in 4 digit Calendar Year (20XX-1999)
Design Life (months)	36	Subcontract design life in months
Instrument Complexity (percentile)	100%	Total instrument suite complexity in percent from 0% to 100%
Total Dry Mass (kg)	3640	Total mass of total spacecraft bus and instruments in kilograms
Total Power (watts)	3350	Total power generated in LOD equivalent beginning of life terms in watts
Bus New Design (Percentile)	65%	Total bus new design in percent from 0% to 100%
Instrument New Design (Percentile)	100%	Total instrument suite new design in percent from 0% to 100%
Year Dollar of Output (000X)	3012	Year dollars of output in 4 digit Fiscal Year (200X)

dividual WBS element costs, then these proportions were applied to the program cost determined by the Satellite Trades tool. Table 9 shows the QuickCost Satellite input parameters. The instrument Complexity and Instrument % New Design inputs were both conservatively input at 100%. The Bus % New Design is also conservative at 65%. Table 10 shows the QuickCost Satellite Trades input parameters. The results of the QuickCost analysis were then plotted with the Bottom-up estimate as shown in Fig.19.

Table 10: QuickCost Satellite Trades Tool Input Table with WFXT Data

Variable	Make inputs in Blue Cells	Variable Units
Destination (earth orbital or planetary) (see note 1)	1.0	0 = earth orbital or 1 = planetary
ATP Date Year (20XX)	2016	Authority to Proceed date in 4 digit Calendar Year (20XX)
Design Life (months)	36	Adjusted design life excluding extended operations in MONTHS
Instrument Complexity (percentile)	100%	Instrument complexity (ability to substitute in percentile terms) FROM 0% to 100% (NOT from 0 to 1.0)
Bus Dry Mass (kg)	3640.0	Mass of spacecraft bus and instruments in kilograms
Instrument Dry Mass (kg) (see note 2)	1520.0	Mass of instruments suite in kilograms
Total Power (Watts)	3350.0	System in LOD equivalent beginning of life terms in watts
Bus New Design (percentile)	65%	Bus new design percentile terms FROM 0% to 100% (NOT from 0 to 1.0)
Instrument New Design Factor (percentile)	100%	Total instrument suite new design in percentile terms FROM 0% to 100%
Structural Material Type	1.0	1= Study A; 2=Aluminum composite; 3=Equivalent Composite in exact mission
Number of Deployables	4.0	Count
Deployables Complexity	1.0	0 = None; 1 = Simple; 2 = Complex
Propellant Mass (kg)	49.0	Propellant mass in kilograms
Thermal Control Type	0.0	0 = Passive; 1 = Active (Active requires assigned Radio-Link (AL) features)
Avionics Material	1.0	0 = Silicon; 1 = Gallium Arsenide
Percentage Active Instruments (percentile)	95	Percentage of the instruments that are active (active, active, none, none)
Spacecraft Volume (cubic meters * 10 ³)	83.00	Theoretical cylindrical volume (length * dia. ²)
Cost Rate (percentile)	75%	
Year Dollar of Output	3012	Year dollars of output in 4 digit Calendar Year (200X)

B.2.2 Bus

The Aerospace Corp. Small Satellite Cost Model (SSCM10) was initially employed to develop the spacecraft bus cost; however, SSCM has a maximum value of 325 W for its beginning of life (BOL) power cost estimating relationship (CER) and the estimated WFXT BOL power is 2,350 W. Hence, the SSCM WFXT electrical power subsystem (EPS) estimate was over-estimated by a factor 5. This and the fact that other WFXT input values; for example, the instrument mass and bus dry mass, are out of SSCMs CER ranges resulted in not using SSCM due to its lack of applicability for this mission. See Table 11 for acceptable SSCM input ranges. Red indicates out-of-range.

Table 11: SSCM Input Table with WFXT Data

Technical Parameter	Range				
	Low	Minimum	Value	Maximum	High
Development Time (ATLO)		22.0	30	92.2	
Development Time (PM/SE/MA)		22.0	30	92.2	
Satellite Wet Mass (ADCS)					
Satellite Wet Mass (ATLO)		110.0	2697	1217.6	121.5%
Satellite Dry Mass					
Spacecraft Bus Dry Mass		52.0	1010	674.0	40.9%
Number of Instruments					
Power Subsystem Mass					
BOL Power (Power)		60.0	2350	325.0	623.1%
BOL Power (Structure)					
BOL Power (Thermal)		109.0	2350	2200.0	6.8%
Structure Subsystem Mass		16.8	456	236.0	93.2%
ADCS Subsystem Mass		2.8	75	58.5	28.2%
Pointing Control		0.006	0.017	3.000	
Propulsion Subsystem Dry Mass		7.1		116.0	
TT&C/C&DH Subsystem Mass		4.7	108	49.8	116.9%
Transmit Power		1.0	5	100.0	
Thermal Subsystem Mass		1.0	38	53.0	

Table 12: NICM Input Table with WFXT Data

Technical Parameter	WFXT value	Particle Sensor Range Maximum	Optical Sensor Range Maximum
Mass (kg)	1638	40	350
Power (W)	663	40	400

B.2.3 Instrument

An attempt was made to use the NASA Instrument Cost Model (NICM IV) particle sensor database to estimate the instrument cost. The WFXT instrument mass and power, 1,638 kg and 663 W, respectively, are significantly greater than the maximum range for NICMs particle sensor CERs. Although WFXT is an x-ray sensor and particles is the appropriate sensor database, an estimate was performed using NICMs optical sensor database to determine if this database was applicable. Using the NICM optical sensing type resulted in an estimate 47% greater than the bottom-up estimate of \$190M due to the WFXT mass being well beyond the maximum range for NICMs optical sensor CERs. For this reason, NICM was not used due to its lack of applicability for this mission. See Table 12 for acceptable NICM input ranges. Red indicates out-of-range.